First palaeointensity data from the cryogenian and their potential implications for inner core nucleation age

Simon J. Lloyd [1], Andrew J. Biggin,[1] Henry Halls[2] and Mimi J. Hill[1]

[1]*Geomagnetism Laboratory, Department of Earth, Ocean and Ecological Sciences, University of Liverpool, Oliver Lodge Building, Oxford Street, Liverpool L69 3GP, UK. E-mail: s.lloyd@liverpool.ac.uk*
[2]*Department of Earth Sciences, University of Toronto at Mississauga, 22 Russell Street, Toronto, ON M5S 3B1, Canada.*

SUMMARY

The timing of inner core nucleation is a hugely significant event in Earth's evolution and has been the subject of intense debate. Some of the most recent theoretical estimates for the age of nucleation fall throughout the Neoproterozoic era; much younger than previously thought. A young inner core requires faster recent core cooling rates and a likely hotter early core; knowledge of its age would be invaluable in understanding Earth's thermal history and total energy budget. Predictions generated by numerical dynamo models need to be tested against such data, but records are currently much too sparse to constrain the event to a precise period of time. Here, we present results from 720 Ma dolerite dykes (and one sill) from the Franklin Large Igneous Province, which fall within a crucial 300 Myr gap in palaeointensity records. This study uses three independent techniques on whole rocks from 11 sites spread across High Arctic Canada and Greenland to produce virtual dipole moments ranging from 5 to 20 ZAm^2 (mean 11 ZAm^2); almost one order of magnitude lower than the present-day field. These weak-field results agree with recent ultralow palaeointensity data obtained from Ediacaran rocks formed ∼150 Myr later and may support that the dynamo was on the brink of collapse in the Neoproterozoic prior to a young inner core formation date.

Key words: Palaeointensity; Palaeomagnetism; Palaeomagnetic secular variation.

1 INTRODUCTION

A fundamental and intensely debated topic in Earth science relates to the question: when did inner core nucleation (ICN) occur? (e.g. Gubbins *et al.* 2014; Biggin *et al.* 2015; O'Rourke & Stevenson 2016; Bono *et al.* 2019). Palaeomagnetic information recorded in rocks can potentially be used to constrain events which occurred in the deep Earth in the ancient past. ICN is expected to have had a major impact on core convection, providing additional power to the geodynamo and moving the primary buoyancy source to much greater depths (Aubert *et al.* 2009). As liquid iron freezes, lighter elements are released, causing compositional convection and the release of latent heat (Nimmo 2015). The location of the dominant buoyancy release changes from a top driven regime at the core–mantle boundary, to one which is bottom driven (Landeau *et al.* 2017). These are competing factors on the resultant geomagnetic field intensity (palaeointensity) observed at Earth's surface because the additional power is being dissipated ∼3500 km further away. Post nucleation, however, it is plausible that we would see an increase in the geomagnetic field intensity at Earth's surface, followed by a higher time-averaged field (Aubert *et al.* 2009; Driscoll 2016). Unfortunately, there are currently insufficient palaeointensity data to provide conclusive tests of such hypotheses.

The current challenge in elucidating long-term observational trends, which might act as a proxy for ICN, has led to wildly varying age estimates and much conjecture. Assessment of existing palaeomagnetic data with new reliability criteria (Q_{PI}; Biggin & Paterson 2014; Kulakov *et al.* 2019) enabled an increase in the Earth's magnetic field between 1.0 and 1.5 Ga to be claimed and hypothesized to have signified ICN (Biggin *et al.* 2015). This was immediately questioned, however (Smirnov *et al.* 2016), and should be considered in light of new palaeomagnetic data gathered from relevant time periods (Sprain *et al.* 2018; Bono *et al.* 2019; Kodama *et al.* 2019; Veselovskiy *et al.* 2019). Furthermore, various numerical dynamo models, using recent increased thermal conductivity estimates in the outer core (De Koker *et al.* 2012; Pozzo *et al.* 2012), tend toward a younger nucleation age of between 500 and 800 Ma (Driscoll & Bercovici 2014; Labrosse 2014; Davies *et al.* 2015). These younger ages are in closer agreement to recent ultralow palaeointensity results obtained using single crystals (as opposed to whole rock samples) of Ediacaran age (Bono *et al.* 2019), hypothesized to be caused by a geodynamo on the brink of collapse immediately prior to ICN. Equally relevant, however, are recent thermal conductivity studies of conflicting values (Konôpková *et al.* 2016; Ohta *et al.* 2016; Zhang *et al.* 2020); this emphasizes the urgent requirement for

more reliable quantitative constraints that palaeointensity data may provide.

Here, we present crucial new palaeointensity data from the mid-Neoproterozoic (∼720 Ma), close in time to when some of the recent dynamo models predict ICN to have occurred (e.g. Labrosse 2014; Driscoll 2016; Landeau *et al.* 2017). These new data are the first to emerge for this time-period, falling in the midst of a critical 300 Myr palaeointensity data gap, with the aim of providing a further constraint on thermal evolution models seeking to address the timing of ICN. The difficulties in obtaining reliable palaeointensity data for the Precambrian are substantial; rocks of the correct age are scarce, the magnetic minerals are likely to have been subjected to reheating, low-temperature oxidation, and other alteration since the time of emplacement. Ideal magnetic recorders should be free from these effects, displaying thermal stability and evidence that the initial thermal remanence magnetization has remained pure, to be confident that the results are unbiased. Previous work (Denyszyn *et al.* 2004) has shown that many of the Franklin dykes (which are the focus of this study) show typical signs of varying hydrous alteration and as such, a conservative approach is adopted here in reporting results, with particular emphasis on assessing reliability and potential bias from alteration and multidomain (MD) effects.

2 FRANKLIN LARGE IGNEOUS PROVINCE (LIP)

The Franklin LIP is a widespread (2.25 M km^2) mafic sill and dyke swarm province in the high Arctic Canada and Greenland (Fig. 1a). The dolerite dykes sampled in this study, from Devon Island, Ellesmere Island and Greenland, are plagioclase-pyroxene cumulates which are petrologically uniform (Denyszyn *et al.* 2004). The dykes are on average 30m wide with well-preserved chilled margins. The surrounding host rocks are high-grade, granitic gneiss of Archean to Palaeoproterozoic age, overlain by flat-lying Palaeozoic carbonate and mudstone. The original palaeodirection study (Denyszyn *et al.* 2009) reports variable amounts of hydrous alteration present in many samples, varying from mild to extensive sericitization of plagioclase. U - Pb ages are available from three sites (BG, CG and QA; Fig 1) and the remaining sites are estimated to be of similar age (721 ± 4 Ma; Denyszyn *et al.* 2009, fig 8). Similar ages have previously been obtained from other Franklin sills and lavas dated at 723 ± 4 and 718 ± 2 Ma (Heaman *et al.* 1992), and dykes 720 ± 8 and 716 ± 4 Ma (Pehrsson & Buchan 1999).

Palaeomagnetic poles obtained from the dykes (mean pole 8.4°N, 163.4°E; Denyszyn *et al.* 2009) are considered robust and agree with multiple previous studies from other regions of the Franklin LIP, such as the Victoria Island sills, Natkusiak volcanics, the Coronation sills and the Thule sills of Greenland (Palmer *et al.* 1983; Park 1994; Buchan *et al.* 2000; Shellnutt *et al.* 2004). The original study (Denyszyn *et al.* 2009) includes a successful baked contact test at site GR and includes reversed-polarity directions (sites SG2 and NU1). Directional results obtained as part of the palaeointensity study carried out here will be compared to the published results to ensure consistency.

A total of 106 standard 1-inch size cylindrical specimens were donated from the original study by Denyszyn *et al.* (2009) for palaeointensity experiments. A total of 17 sites are included in this study, with samples per site ranging from 3 to 13. The locations of the 17 sites are shown in Fig. 1(a) and the corresponding site mean palaeomagnetic directions from Denyszyn *et al.* (2009) are shown in Fig. 1(b).

3 METHODS

3.1 Rock magnetic experiments and microscopy

Hysteresis parameters were obtained alongside thermomagnetic curves of the saturation magnetization (Ms-T) and isothermal remanent magnetization (IRM) acquisition curves using a Magnetic Measurements Ltd Variable Field Translation Balance (VFTB) which was housed in a magnetically shielded room. All experiments were undertaken in ambient air. Due to the limited availability of material, an average of two powdered subsamples with masses in the order of 150 mg were used to represent each site.

The magnetic susceptibility of representative specimens (one or two per site) was measured using a MFK1-FA Kappabridge susceptometer with CS-3 furnace (AGICO) to high temperature (up to 700 °C) in an argon gas atmosphere. Several partial curves were measured with increasing maximum temperatures.

A viscous remanent magnetization (VRM) experiment (Prévot 1981) was carried out on 35 samples to identify their viscous coefficient (v), where $v = \frac{|\overrightarrow{M_1} - \overrightarrow{M_2}|}{|\overrightarrow{M_1} + \overrightarrow{M_2}|}$.

Samples were orientated with the Earth's field in the Z− position for three weeks (M_1), and the same in the Z+ position (M_2) followed by 3 weeks in a zero-field environment; declination, inclination and intensity were measured after each stage.

Thin sections (one from each of four sites) were selected to represent a mixture of magnetomineralogies, as determined by rock magnetic results. These were examined under a scanning electron microscope (SEM) using electron-dispersive X-ray spectroscopy (EDS) spot analyses for quantitative element identification.

3.2 Absolute palaeointensities

All original one-inch specimens were halved to make 212 separate A and B half-inch specimens. Microwave specimens which are smaller were drilled from a half-inch specimen. Specimen names consist of the site identifier; first two letters (or two letters and a number plus a dash in the case of sites SG2 and SG3), followed by the core number; a dash then separates the specimen number and whether it is from the A or B half of the original provided specimen. For example, specimen BB5-1A is from site BB, core 5, specimen 1A. Microwave specimens have an additional number at the end where more than one specimen is from the same half inch core e.g. BP6-1B3 indicates that this is the third microwave specimen obtained from specimen 1B, core 6, site BP. Sister specimens are defined as adjacent specimens from the same core, or microwave specimens from the same half-inch specimen. These are compared where possible using a multiple technique approach to assess palaeointensity, which can increase the experimental success rates and allow for cross-technique comparisons.

Three main methods were used here; the Shaw double heating technique (DHT; Tsunakawa & Shaw 1994; Yamamoto *et al.* 2003), thermal Thellier (Thellier & Thellier 1959; Tauxe & Staudigel 2004) and the microwave method (Walton *et al.* 1992; Hill *et al.* 2002). All thermal Thellier and Shaw-DHT measurements were performed using a RAPID 2G superconducting rock magnetometer in a magnetically shielded cage where the residual field was less than 100 nT. The microwave experiments were carried out using the 14.2 GHz Tristan microwave palaeointensity system at the University of Liverpool.
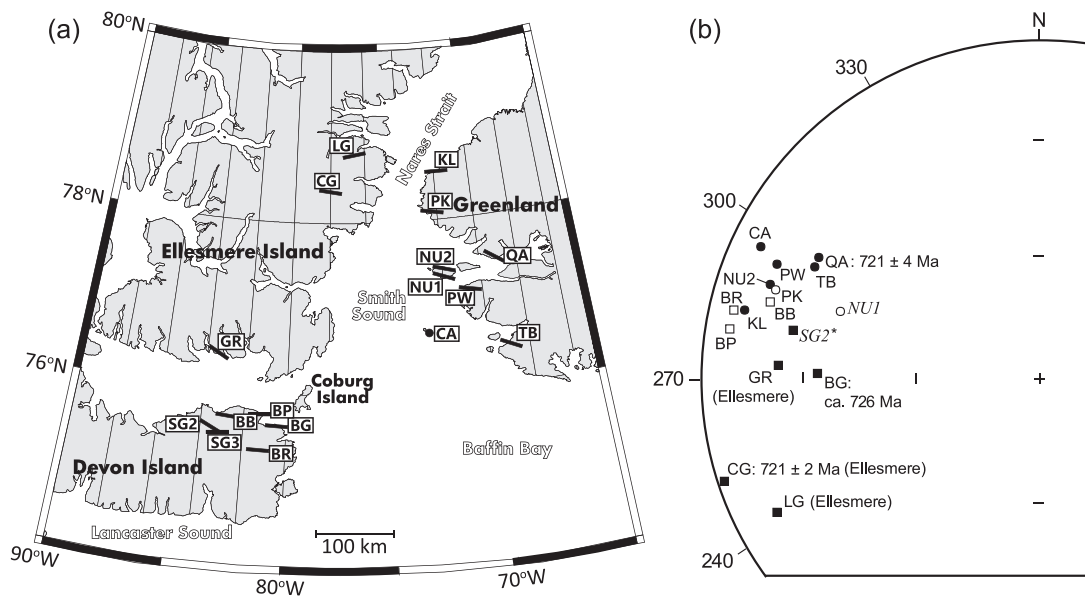
Figure 1. (a) Map showing the position of the Franklin dykes and one sill used in this study. Dykes (black lines) are identified by their site names (in boxes). (b) Equal-area stereoplot of the quality-filtered, site-mean palaeomagnetic characteristic remanence magnetization directions obtained by Denyszyn *et al.* (2009) relating to the Franklin dykes and sill (site CA) in this study. Circles, Greenland data; squares, Canada data; solid, lower hemisphere; open, upper hemisphere. Italics indicate reversed polarity directions (sites NU1 and SG2). Asterisk indicates that directions were taken with magnetic compass only. Where ages are available these are given beside the site. [(a) and (b) are adapted from Denyszyn *et al.* (2009).] Site SG3 is not shown in (b) as its directions are transitional and was not included in the main table of the original paper by Denyszyn *et al.* (2009), although its location is identified in (a).

The Shaw-DHT experiments (Tsunakawa & Shaw 1994; Yamamoto *et al.* 2003) were undertaken using varying laboratory protocols to improve robustness of results. At a basic level, a palaeointensity can be derived by comparing the demagnetization spectra of a natural remanent magnetization (NRM) with a laboratory induced thermal remanent magnetization (TRM). Any alteration that occurs due to the laboratory heating is estimated by comparing the demagnetization spectra of an anhysteretic remanent magnetization (ARM) imparted prior to, and post laboratory heating; the difference in ARM is a direct result of the alteration and is applied as a correction to the TRM. The ARM corrections are then performed again on a second laboratory heating in order to recover the initially imparted known field, thereby acting as a reliability check on the corrections used for the palaeointensity calculation (the DHT part).

All specimens were heated in a vacuum at a rate of 60 °C min^{-1} to 500 °C, followed by 5 °C min^{-1} to 610°C where they were held at temperature before cooling. A total of 33 specimens were held at 610 °C for 45 min for the first and the second heating. Laboratory TRM was imparted in a 20 µT DC field along the *z*-axis of the samples while ARM was imparted using a 100 µT bias field. A further 16 specimens were held for 20 (60) min the first (second) heating with a laboratory TRM of 20 µT DC field and an ARM bias field of 70 µT. The purpose for changing the input variables was to increase the robustness of the results by minimizing any input biases. Specimens were stepwise demagnetized using alternating frequency (AF) steps of 5–10 mT to a maximal field of 100 mT. ARMs were imparted at 100 mT to coincide with the maximum AF demagnetizations.

Two Shaw-DHT experiments included the use of low-temperature demagnetization (LTD), which is known to preferentially target remanence carried by multidomain grains (Yamamoto *et al.* 2003). LTD specimens were soaked in liquid nitrogen in a plastic Dewar

for 10 min and then removed and allowed to warm to room temperature in a zero field for 60 min. In the first instance, 16 specimens from 10 sites were subjected to a full Shaw LTD-DHT experiment with the addition of a non-LTD ARM (ARM$_0$); the two ARM$_0$ treatments were compared in order to quantify the MD component of remanence. We also compared Shaw-DHT results from two separate experiments, where one set of samples were treated with LTD and one set without. These were carried out on sister samples to check for any systematic bias that the treatment may have on the results. Thermal Thellier experiments were used to measure 36 specimens from ten sites; these consisted of a sequence of paired heatings in air, to a set of increasing temperatures. The IZZI+ protocol was used (Tauxe & Staudigel 2004) which alternates the zero-field and infield steps, with partial thermal remanent magnetization (pTRM) checks after every two step pairs. The sequence of steps was repeated up to an average of 600°C, with an infield laboratory bias field of 20 µT. A pre-treatment 5mT AF cleanse was used in some experiments and compared to those without the treatment.

A total of 26 further experiments were carried out using the microwave system. Small cylindrical cores (5 mm diameter) are centred in the resonant cavity, where the microwave field couples with the magnetic system to demagnetize the sample. The IZZI+ protocol (as used with the thermal Thellier experiments) was used with an additional requirement that the ChRM make an angle of at least 45° with the lab field; this achieves a compromise between minimizing any non-ideal behaviour arising from multidomain effects while also being able to detect its presence (Hawkins *et al.* 2019). The microwave method has been demonstrated to produce equivalent results to thermal Thellier-style experiments (Biggin *et al.* 2007), and in some cases, improved results (Grappone *et al.* 2019).

To further check the reliability of the successful palaeointensity estimates, we assessed potential biases related to anisotropy

of remanence. We compared the angular difference between the last pTRM step used for the palaeointensity determination and the applied field direction (γ).

Palaeointensity results were quantitatively assessed using selection criterion parameters set out in the standardized palaeointensity definitions (Paterson *et al.* 2014) and are similar to those used in other studies (Yamamoto *et al.* 2003; Shcherbakova *et al.* 2017a). For all experiments:

(1) A maximum angular deviation; MAD < 10 °

(2) The angle between an anchored and unanchored fit of the directional data to the origin of an orthogonal vector plot; α < 15 °

(1) Number of measurements used for palaeointensity determination (N) $\geq$ 4.

For Shaw (LTD) DHT experiments:

(1) The linear segment of the palaeointensity slope should include the maximum AF step identified as characteristic remanence, thereby reducing ambiguities in the calculation of palaeointensity.

(2) The R^2 correlation (rN) of the palaeointensity slope$_N$ (demagnetization spectra NRM/ TRM$_1$∗; Yamamoto *et al.* 2003) > 0.990

(3) Slope$_T$ (demagnetization spectra TRM$_1$/ TRM$_2$∗; Yamamoto *et al.* 2003) = 1 ± 0.05 (Class A result) and ± 0.10 (Class B result)

(4) The R^2 correlation (rT) of the slope$_T$ > 0.990

(5) Fraction of coercivity used in palaeointensity determination (fN) $\geq$ 0.25 (Class A result) and $\geq$ 0.20 (Class B result)

3.3 Thellier IZZI+ (thermal and microwave)

1) NRM fraction used for the best fit on the plot of NRM lost versus TRM gained (Arai diagram) determined entirely by vector difference sum calculation; FRAC $\geq$ 0.35 (Class A result) and $\geq$ 0.25 (Class B result).

2) The slope of the best-fitting line of the selected TRM and NRM points on the Arai plot, or scatter parameter; β < 0.1.

3) Number of pTRM checks > 2.

4) The maximum absolute difference produced by a pTRM check, normalized by the total TRM (dCK) $\leq$ 20 per cent.

5) The maximum absolute difference produced by a pTRM check, normalized by the length of the best-fitting line ($DRAT$) $\leq$ 15 per cent.

6) The sum of the absolute pTRM difference ($CDRAT$) $\leq$ 20 per cent.

7) The curvature of the linear section of a selected palaeointensity slope (k') $\leq$ 0.48

4 RESULTS

4.1 Rock magnetic and microscopy

Rock magnetic and microscopy results are presented in Figs 2 and 3 and Supporting Information Figs S1 and S2. Hysteresis parameters of representative specimens are consistent with grain populations located predominantly in the so-called pseudo-single-domain state and are summarized in a Day plot (Day *et al.* 1977; Fig. 2a). A small number of subsamples (QA11-1, QA4-1A & BB7-5A) locate close to the MD section; however, samples from site QA also locate in the main cluster of results. VRM coefficients (v) are generally acceptable (<10 per cent), however, higher values of 14 per cent or greater are observed from sites GR, LG, PK, BB, and samples from site BG exceed 100 per cent (Fig. 2b).

Ms-T curves (Fig. 2c) indicate single Curie temperatures of between 550 and 590 °C suggesting that the main magnetic carriers are low titanium-titanomagnetite (Dunlop *et al.* 1998). Curves are separated according to their reversibility at room temperature with a 20 per cent threshold, however, consistent behaviour is observed across all specimens and sites with only small differences in reversibility. IRM curves saturate by 180 mT (Fig. 2d) with no indication of high coercivity minerals present suggesting that the remanence is most likely carried by (titano) magnetite.

Susceptibility on heating (k–T) curves show a range of reversibility and suggest equivalent Curie temperatures to Ms-T curves. Many samples show no clear evidence of alteration (Fig. 2e), however, as expected from rocks of this age, some k–T curves are less reversible and show a slight inflection at ∼300 °C (Fig. 2f), indicating mild low-temperature oxidation; these are likely in response to reported hydrous alteration (Denyszyn *et al.* 2009); these require more careful handling (diagrams of additional k–T curves are found in Supporting Information Fig. S1).

SEM results show two distinct opaque grains, indicating that samples from a particular site would either comprise of sizes ∼ 5 μm (Figs 3a and b) or ∼100 μm (Figs 3c and d). Larger grains appear to show alteration textures consistent with low-temperature oxidation. Grains in one sample (Fig. 3d) had also undergone oxyexsolution, likely during primary cooling, such that lamellae of ilmenite and Ti-poor titanomagnetite were visible. Details of the EDS spot analysis is found in Supporting Information Fig. S2. Although these much larger grains are not the stable remanence carriers, potential alteration effects in samples from these sites are considered in detail, later in the manuscript.

The rock magnetic and microscopy results suggest that approximately half of the 17 sites (BP, CA, NU1, NU2, PW, SG3, QA and TB) show promise for producing reliable palaeointensities and that the remainder have either been subjected to various degrees of alteration or are likely to suffer from alteration in any laboratory heatings.

4.2 Absolute palaeointensities

Pilot Shaw-DHT experiments were combined with preliminary rock magnetic results to identify the most suitable sites and specimens for palaeointensity analysis. Sites BB and PK were rejected after this stage due to poor VRM coefficients, uninterpretable demagnetization of the NRM or failed palaeointensity experiments (Supporting Information Table S1). Successful palaeointensity results were obtained using all three methods, from 10 out of 16 sites, ranging from 1.1 to 9.9 μT. Three of these sites (BG, BR and GR) yield less than three individual results per site and are not used to calculate a VDM. Site-mean palaeointensity estimates were determined from the unweighted average of successful results from all methods from a given site. Specimen level results are found in Supporting Information Tables S1–S3 for Shaw-DHT, Thermal Thellier IZZI+, and microwave IZZI+ respectively and representative sample plots are shown in Figs 4 and 5. A summary of all successful palaeointensity results is presented in Table 1.

The Shaw-DHT method produced the most successful palaeointensities with 24/59 specimens yielding positive results across nine sites (Supporting Information Table S1 and Figs 4a, d and g). Shaw (LTD)-DHT results range from 1.1 to 9.9 μT (4.8 μT mean). A comparison of LTD treated ARM versus non-LTD treated ARM (Supporting Information Fig. S3) shows that LTD-prone remanence
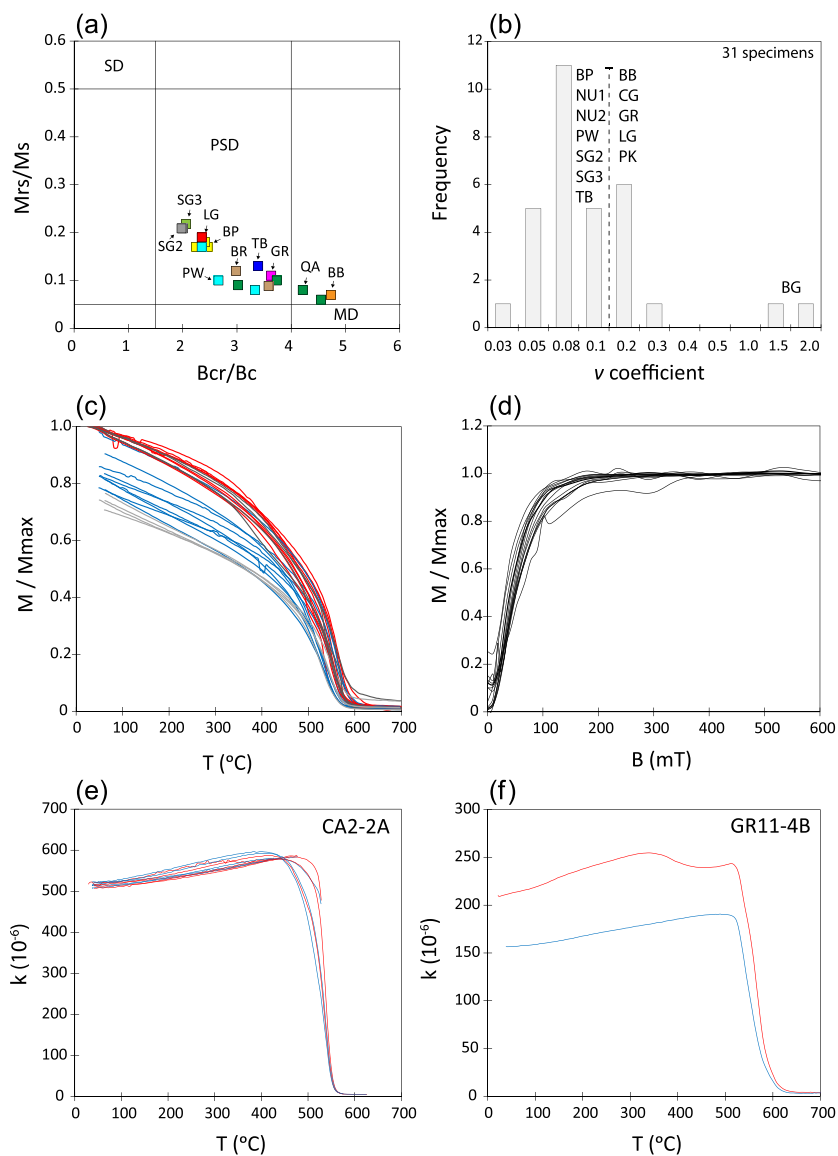
Figure 2. (a) The Day plot of the hysteresis parameters (Day *et al.* 1977). Mrs/Ms, remanent saturation magnetization/saturation magnetization; Bcr/Bc, remanent coercive force/coercive force. (b) Histogram of VRM results. The dashed line separates sites according to whether they have v coefficients of less or more than 0.1 (10 per cent). (c) Accepted Ms-T curves; red, heating; blue, cooling; rejected Ms-T curves; dark grey, heating; light grey, cooling. M/M$_{MAX}$, magnetization normalized by the maximum value; *T*, temperature. (d) IRM curves normalized. (e and f) Representative high-temperature/susceptibility reversible (e) and non-reversible (f) curves; *k*, susceptibility; *T*, temperature. Diagram (f) also shows an inflection of ∼300 °C. Red lines, heating curve; blue lines, cooling curve.

was completely removed by 25 mT for all specimens. In addition, no systematic intensity differences were observed between specimens which underwent LTD and those that did not (Supporting Information Fig. S4); most sister specimen results are within 1–2 µT. Slope$_{A1}$ (ARM$_0$/ARM$_1$), which is a measure of ARM alteration, indicates that a mean correction of 28 per cent was applied. A slight correlation was observed in which larger corrections (slope$_{A1}$ further from 1) are associated with higher palaeointensity results (Supporting Information Table S1). Changing the first heating duration from 45 to 20 min, and the second heating from 45 to 60 min, in the Shaw-DHT experiments, produced a *slope$_T$* further from unity in sister samples but did not appear to affect the palaeointensity results. We therefore allow for a slightly relaxed *slope$_T$* criterion (see selection criteria, Section 3.2) and define these results as class B.

Additionally, class B results are also defined in results with a single relaxed criterion (fN ≥ 0.2; Supporting Information Table S1); the inclusion of these results does not significantly affect the within-site scatter and they are in close agreement with results using the stricter criterion. Where a relaxed fN is accepted, the minimum number of steps required in the palaeointensity slope (*N*) is increased from four to six.

Unsuccessful specimens typically failed to meet criteria associated with the correlation of the NRM-TRM slope or due to a lack of reproducibility (*slope$_T$* criterion); in some cases, the characteristic directions were also not sufficiently well-defined. The directions obtained from the successful Shaw-DHT palaeointensity results here are consistent with those from the original study (Denyszyn *et al.* 2009; Supporting Information Table S1).
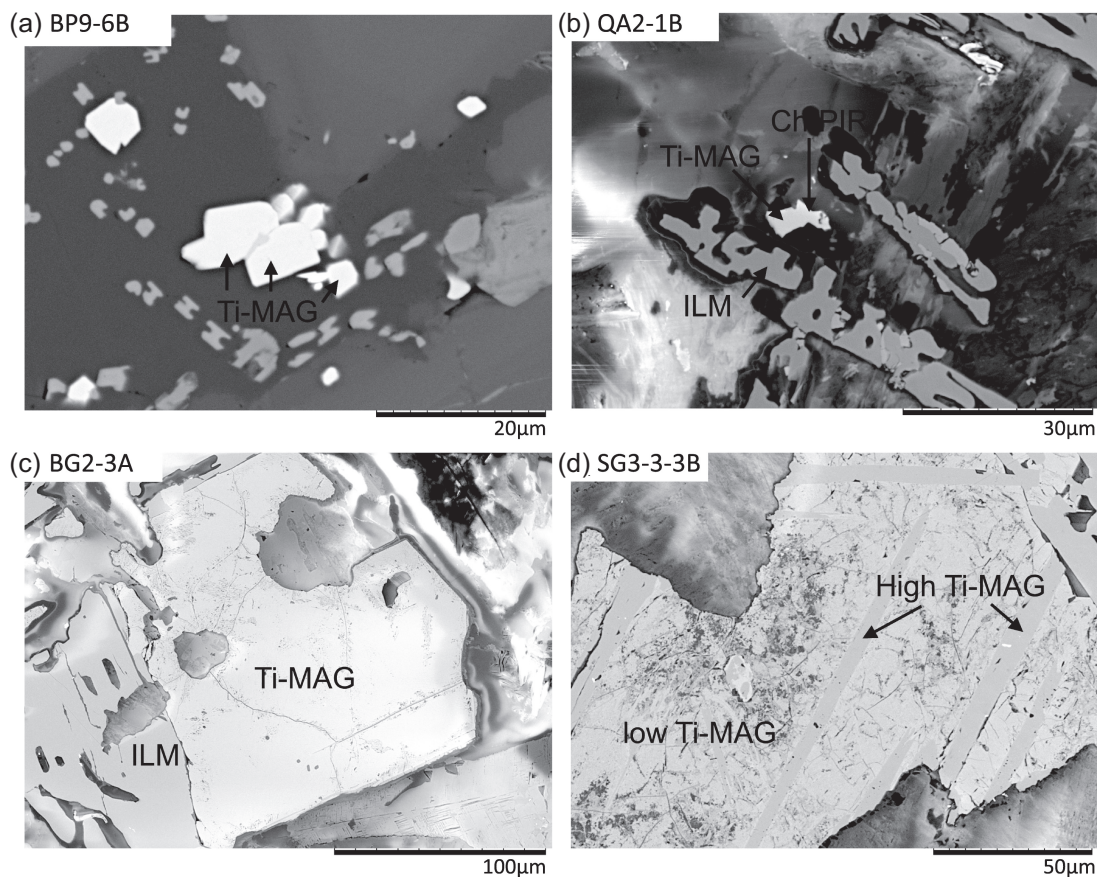
Figure 3. Examples of mineral fabrics observed using a scanning electron microscope from four sites. (a and b) Specimens BP9-6B, and QA2-1B showing fine low-Ti titanomagnetite grains which appear pristine. (c) Specimen BG2-3A shows much larger ilmenite and low-Ti titanomagnetite grains (∼100um), with cracks consistent with alteration. (d) Specimen SG3-3-3B shows large, altered grains with further evidence of alteration. Ti-MAG, Titanomagnetite; ILM, Ilmenite, Ch-PIR, Chalcopyrite.

Thermal Thellier and microwave experiments produced 5/ 36 and 10/ 26 accepted results (Supporting Information Tables S2 and S3), respectively. The results are similar to those of the Shaw experiments, with Microwave ranging from 3.5 to 6.7 µT (4.5 µT mean) and thermal Thellier from 1.0 to 7.4 µT (4.6 µT mean). In some accepted results, Arai diagrams display two-slope behaviour, the change in which corresponds to a change between secondary and characteristic remanence direction (e.g. Figs 4f and 5b), rather than requiring multidomain effects to explain (Smirnov *et al.* 2017; Hawkins *et al.* 2019). The high-temperature sections of most two-slope Arai plots correspond to the primary remanence, as observed in the associated orthogonal diagram; this is particularly apparent in the very low result (1.6 µT) of specimen BG1-4B (Fig. 5a). An instance where this is slightly more difficult to discern is observed in the Arai diagram for specimen BP5-1A (Fig. 5b); here, a prominent two-slope is associated with a less clear change in direction, however, a maximum of two earlier steps could be interpreted as primary and would not change the result. A straight-line fit from 20 to 565 °C was also determined for this sample and would only alter the palaeointensity result from 1 to 2.6 µT (Supporting Information Fig. 5).

Common reasons for failure in microwave and thermal Thellier IZZI experiments, associated with multidomain behaviour and alteration of the magnetic carriers, are excessive 'zigzagging' and failure of pTRM checks in Arai-plots (Supporting Information Fig. S6). Several specimens did not produce interpretable Arai-plots;

these were mostly from specimens where no AF pre-measurement steps were applied. A relaxed criterion is used ($FRAC \geq 0.25$) in a class B result for microwave specimen QA4-1A2. The results from a direct comparison of eleven sister specimens from Shaw-DHT and microwave methods are in good agreement (Supporting Information Fig. S7), producing an R^2 correlation of 0.63; this is improved by the removal of a single outlier to $R^2 = 0.90$.

The highest success rate is achieved from the Shaw-DHT experiments, most likely because the method applies a correction for any alteration caused by heating in the laboratory. Shaw type experiments are also expected to be less prone to domain state effects than Thellier-type because they use a single full heating which means that Thellier's laws of independence, additivity and reciprocity are less likely to fail. Microwave Thellier experiments are also more successful than thermal; this may be because the microwave / magnon system (analogous to heat/phonon) may reduce bulk specimen heating (e.g. Hill & Shaw 2000; Suttie *et al.* 2010). The thermal Thellier results are in agreement with, and supported by, the partial reliance on non-Thellier data, which come from two separate and well-documented palaeointensity methods (Tsunakawa & Shaw 1994; Hill & Shaw 1999; Hill & Shaw 2000; Yamamoto *et al.* 2003). Results were also tested using a stricter set of selection criteria; this had no notable effect on site-mean results other than to decrease the success rates slightly (Supporting Information Table S5).

A consistently weak field is recorded with successful results obtained from eleven sites and by all three palaeointensity methods
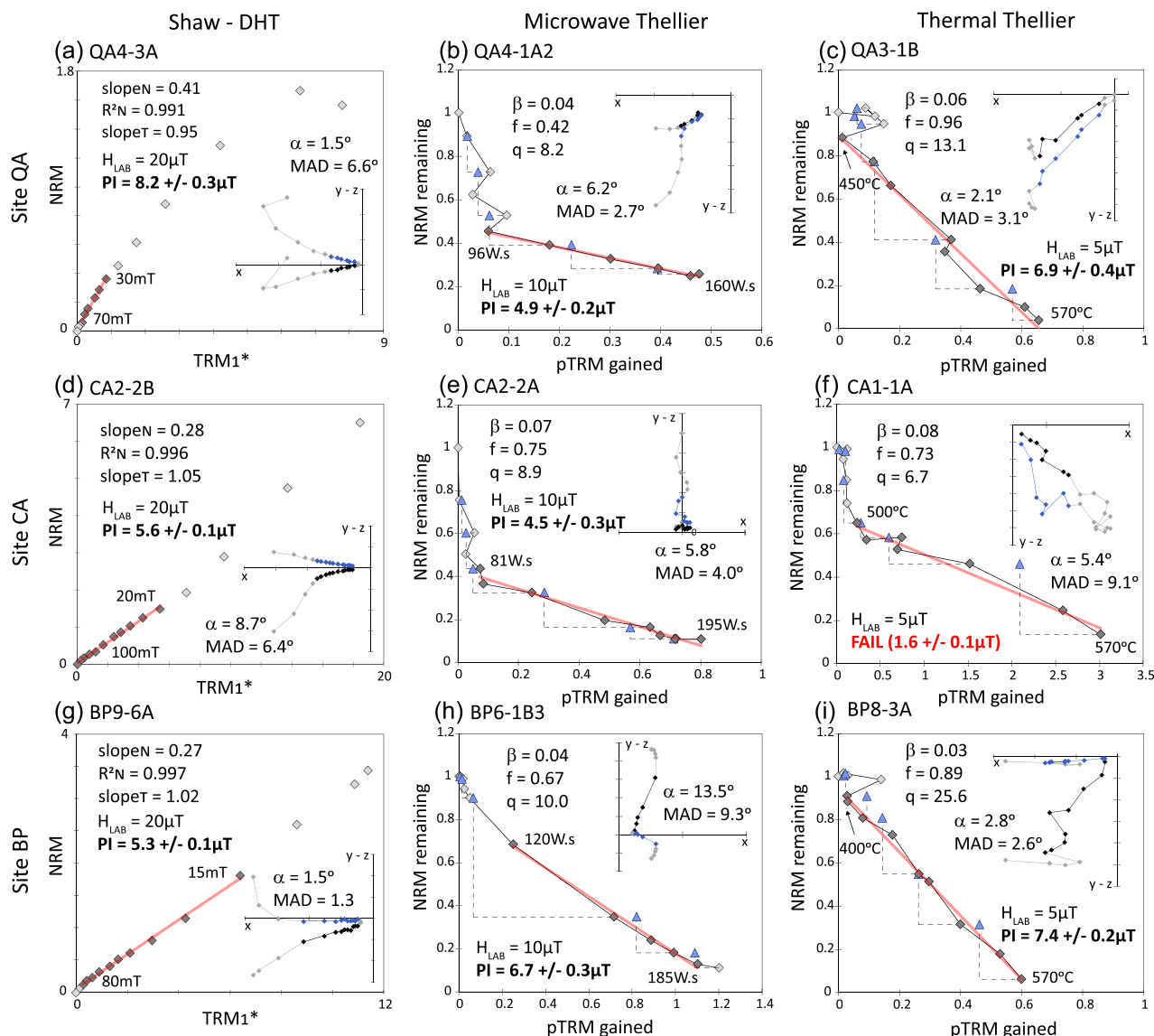
Figure 4. A selection of Arai plots from the microwave and thermal Thellier experiments, and Shaw pseudo-Arai plots (units 10^{-6} Am^2). Each column includes only results from the same method; each row includes only results from the same site. CA2-2A and CA2-2B are sister specimens. Red line, best-fitting line for palaeointensity points used; blue triangles, pTRM checks; dashed lines, link the pTRM check to the position that the check was carried out. Dark grey points are used in palaeointensity determination; light grey points are not used. Orthogonal plot data corresponding to (pseudo)-Arai plots are highlighted in black and blue with the remaining points greyed out. An explanation of the selection criteria is given in Section 3.2.

(Table 1). Site-mean inclinations (Denyszyn *et al.* 2009) were used to calculate virtual dipole moments (VDMs) that ranged between 3.6 and 19.3 ZAm^2. Four of the eleven site means are defined by fewer than three palaeointensities, consequently no VDM is determined for these sites; they are retained for comparison only.

5 DISCUSSION

5.1 Palaeointensity reliability

Rock magnetic and palaeointensity results largely concur; sites associated with *k–T* curves which share common features such as slight inflections at ∼300 °C (CG, LG, KL; Figs 3h–j) fail to produce any successful palaeointensities. Sites associated with high (>10 per cent) VRM coefficients (GR, LG, BG) also fail to

produce successful palaeointensity results with the exception of one result from site BG and one from GR, neither of which are used in the final determination of VDM results because the number of successful results from these sites are less than three. SEM micrographs depicting fine grains are from two sites with the highest palaeointensity success rates (BP and QA) in contrast with those with large, altered grains (sites BG and SG3). These correlations suggest that the applied palaeointensity selection criteria were successful in filtering out unreliable recorders. A small number of specimens (e.g. those from site QA) have hysteresis parameters that suggest they were some of the least suitable (Fig. 2a) but were retained on the basis of their *k–T* curves and SEM observations (Fig 3) and gave high-quality palaeointensity results.

Due to vortex domain-state bulk properties and the potential of field underestimation from using high-temperature segments of
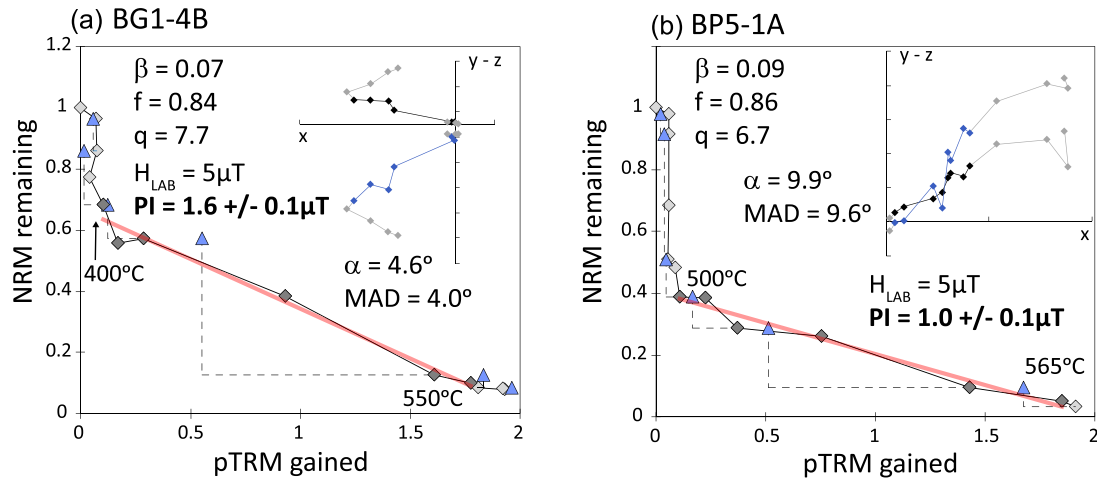
Figure 5. (a and b) Additional thermal Thellier Arai diagrams with associated orthogonal plots. See selection criteria (Section 3.2) and caption in Fig 4 for further details.

two-slope Arai diagrams, careful scrutiny of the data is applied to determine the possibility, if any, of MD bias in the final palaeointensity estimations. We find that there are numerous lines of evidence to suggest that the successful results are free from such bias:

There is reasonable evidence (high *FRAC* with low β, low curvature, domain state independent method) that the final presented estimates are not significantly biased by multidomain behaviour during the experiment; and as such, we award a pass in our assessment of the quality of palaeointensity (Q_{PI}; Biggin & Paterson 2014) for the MD criterion; evidence that the final estimate was not significantly biased by multidomain behaviour. All sites are assigned Q_{PI} scores which range between 5 and 9 (Table 1 and Supporting Information Table S6). Only two sites (BG and QA) are associated with specific radiometric ages but as part of a single large igneous province, all dykes from this study can reasonably be assumed to have been emplaced over just a few million years (Bryan & Ernst 2008) and their palaeointensities are derived from an interpreted primary component of remanence, which satisfies the AGE criterion; a reliable age and palaeomagnetic behaviour consistent with palaeointensity derived from a primary component of remanence.

All sites also pass ALT criterion; reasonable evidence that the final estimate was not significantly biased by alteration occurring during the experiment. Any steps associated with alteration were identified by pTRM checks and excluded, or corrected using the ARM technique (Shaw method) which was itself subsequently checked. SEM images indicate that for two sites (BP and QA), the remanence is carried by unaltered grains that may reasonably be assumed to have formed during primary cooling, and therefore satisfy the TRM criterion; evidence that the component of remanence in the bulk of samples is likely a TRM, whereas the poor quality observed in thin sections from sites SG3 and BG are cause for failure. We adopt a cautious and strict approach to the remaining sites where no SEM evidence is available; these sites are also are not awarded a pass, although there is no reason to expect at least some of these sites would pass, particularly the sites with the highest quality rock magnetic results.

The low field values made it difficult to pass the STAT criterion; a minimum of 5 individual sample estimates per unit with low dispersion, as they are associated with a higher relative standard deviation. It is worth highlighting that the absolute standard deviations are small, ranging between 0.2 and 2.6 µT. All sites pass

the ACN criterion; the final estimate was not significantly biased by anisotropy of TRM, cooling rate effects, and nonlinear TRM effects. Calculations of γ-values indicate minimal anisotropy; cooling rate is considered unproblematic because the specimens were collected from dyke margins, with rock magnetic evidence of vortex-state grains, and finally, nonlinear TRM effects were tested by using several bias fields in the multiple palaeointensity experiments.

5.2 Significance of results for the geodynamo

While we note that palaeointensity estimates from seven rapidly cooled units are unlikely to provide a strong averaging of secular variation, we nevertheless highlight their consistent low values across well-dispersed sites (and methods), ranging from 1.0 to 9.9 µT with a median of 4.4 µT. We therefore consider it very likely that the time-average field was low at this time, noting also, that the presence of several reversed-polarity directions suggests at least one reversal of the geomagnetic field has been captured. These new data allow the first characterization of the geomagnetic field from any time within the mid-Neoproterozoic.

An analysis of the virtual geomagnetic pole (VGP) dispersion of the Franklin LIP data from Denyszyn *et al.* (2009) yields Angular dispersion of 11.6° ± 3.7 ° at a palaeolatitude of 7 °N ($N = 23$). This is approximately equivalent to that expected from analysis of the PSV10 data set of volcanics from the last 10 Myr (Cromwell *et al.* 2018; Doubrovine *et al.* 2019; Supporting Information Section S3 and Table S4). This supports the Franklin LIP being emplaced during a time period when the average axial dipole dominance was similar to recent times (Biggin *et al.* 2020) despite the substantially reduced average dipole moment.

We provide an interpretation of the most current palaeointensity global database for the 300 – 2500 Ma period. All data is taken from the PINT database (v.2015.05; http://earth.liv.ac.uk/pint/) (Biggin *et al.* 2015). Data older than 500 Ma has been assessed according to the Q_{PI} criteria and assigned scores (Biggin *et al.* 2015). A filter has been applied to all of this data to only include those with a Q_{PI} score of 3 or more. In addition, a limit is applied so that a minimum of three samples per cooling unit have been used to calculate the VDM. These generalized minimum criteria are accompanied by the removal of results of the ~1300 Ma Gardar lava flows in Greenland (Thomas & Piper 1992, 1995; Thomas 1993) believed now to be

Table 1. Palaeomagnetic Results.

Site	U/Pb date (Ma)	Type	Lat (°N)	Lon (°W)	Dec (°)	Inc (°)	Ndir	k	a95 (°)	F (μT)	6F (μT)	NPI	N_{mic}	N_{Shaw}	N_{Thel}	VDM (ZAm²)	Q_{PI}
BB	–	Dyke	75.7	83.0	286.0	–18.0	9	91	5.4	1.6	–	–	–	–	–	–	–
BG	726 (±24)	Dyke	75.6	80.2	271.3	34.5	7	24	12.6	5.5	2.5	1	1	–	1	*3.6*	5
BP	–	Dyke	75.8	81.3	279.2	–7.5	9	70	5.2	4.9	0.3	7	1	3	3	14.1	8
BR	–	Dyke	75.5	81.6	282.6	–7.5	7	226	4.0	3.9	1.8	2	2	–	–	*12.6*	6
CA	–	Sill	76.7	73.2	295.4	9.3	5	234	5.0	–	–	4	2	2	–	9.9	6
CG	–	Dyke	78.3	77.1	251.9	1.8	7	46	9.0	2.3	–	–	–	–	–	–	–
GR	–	Dyke	76.4	83.0	272.9	23.3	8	190	4.0	–	–	1	–	1	–	*5.6*	6
KL	–	Dyke	78.7	70.7	283.0	10.9	8	74	6.5	–	–	–	–	–	–	–	–
LG	–	Dyke	78.7	75.7	243.1	13.7	7	91	6.4	–	–	–	–	–	–	–	–
NU1	–	Dyke	77.4	71.6	108.3	37.7	8	59	7.3	–	–	–	–	–	–	–	–
NU2	–	Dyke	77.4	71.5	289.9	16.3	8	123	5.0	4.4	–	1	–	1	–	*11.0*	6
PK	–	Dyke	77.9	72.2	288.7	–18.5	7	132	5.3	–	–	–	–	–	–	–	–
PW	–	Dyke	77.2	70.8	293.6	15.9	7	144	5.1	3.1	0.3	4	1	4	–	7.9	6
QA	720 (±3)	Dyke	77.5	68.9	298.8	26.1	6	106	6.5	8.1	0.8	5	1	3	1	19.3	9
SG2	–	Dyke	75.7	84.0	101.2	–26.4	6	103	6.6	2.4	1.3	4	2	2	–	5.7	6
SG3(T)	–	Dyke	~75.70	~84.00	68.9	61.4	10	123	4.4	2.9	0.2	3	–	3	–	4.8	5
TB	–	Dyke	76.5	69.2	296.5	26.4	9	37	8.6	6.4	2.1	7	2	5	–	15.2	6

Note: A summary of palaeomagnetic results. Dec (°), magnetic declination; Inc (°), magnetic inclination; Ndir, number of specimens used to determine the mean direction; *k*, the Fisher precision parameter; a95, 95 per cent confidence limit on the mean direction; *F*, field intensity; 6*F*, absolute standard deviation; NPI, number of palaeointensity results; N_{mic}, N_{Shaw} and N_{Thel} are the number of results for each method; VDM, virtual dipole moment; Q_{PI}, quality score of palaeointensity; ~, SG3 site lat & long estimated from Denyszyn et al. (2009) map. Directions are from Denyszyn et al. (2009). Italics denote sites with *n* < 3; (T), Transitional. Site-mean palaeointensity results are unweighted average of all successful results from all methods for a given site.
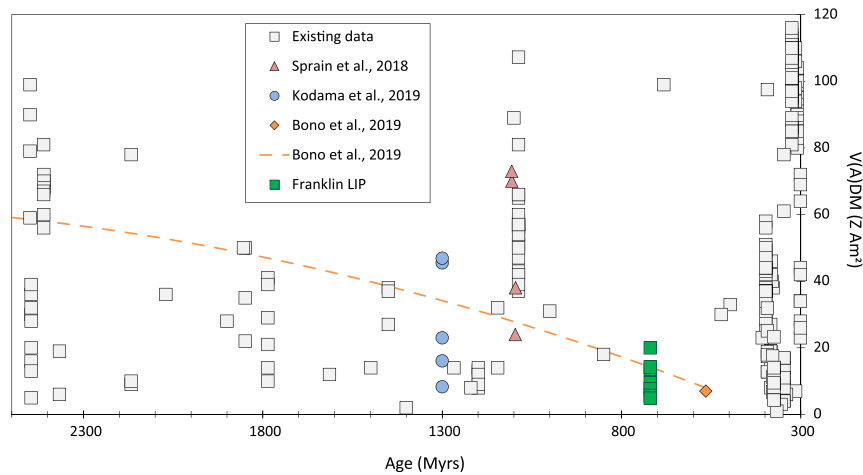
Figure 6. Virtual (axial) dipole moment data (V(A)DM) through time (300 – 2500 Ma). Data taken from the PINT database (v.2015.05; http://earth.liv.ac.uk/pint/; Biggin *et al.* 2015) with the addition of recent data from Shcherbakova *et al.* 2017, Sprain *et al.* 2018, Hawkins *et al.* 2019, Kodama *et al.* 2019 and Bono *et al.* 2019. The dashed line is the weighted second-order polynomial regression of Precambrian field strength data by Bono *et al.* 2019. Data >500 Myr has been filtered to exclude VDM data with $Q_{PI} < 3$, N <3.

over-estimations of the palaeofield, and have been superseded by (Kodama *et al.* 2019).

These new data provide an additional test of recent numerical models and statistical hypotheses which suggest alternative ages for ICN spanning more than 300 Ma (Labrosse 2014; Driscoll 2016; Landeau *et al.* 2017). Driscoll (2016) predicts that the geodynamo entered a weak-field state during the period prior to ICN (~1000–650 Ma), following a dipole high (1.0–1.7 Ga). Palaeointensity data do not support the long-term dipole high for the early part of this interval (Fig. 6), with the only reliable high VDM estimates (>60 ZAm^2) recorded at ~1.1 Ga from the Midcontinent Rift (Kulakov *et al.* 2013, Sprain *et al.* 2018). However, the hypothesis provided by Driscoll for the long-term intensity trend of Earth history fits well with these most recent observations. The unique high at ~1.1 Ga is otherwise difficult to explain apart from that it may result from substantial variation about the long-term trend because of changing core–mantle boundary conditions, despite the decline in thermal convection reducing the core to a low power state.

Biggin *et al.* (2015) hypothesized that nucleation may be linked to an increase observed in the average VDM between 1 and 1.5 Ga. Our results do not support this hypothesis but, similarly, cannot yet rule it out. There remains a severe paucity of data in the interval 600–1100 Ma and, considering the fluctuations that are observed in the Phanerozoic geomagnetic field (Biggin *et al.* 2012), it is possible that any of the Precambrian studies may capture a temporally or spatially limited anomaly that is not representative of the very-long-term average.

Additional complications may exist in using palaeointensity as a proxy for ICN. Palaeointensity records are currently too sparse to allow a meaningful time-series analysis of variations occurring even on 100 Myr timescales through Precambrian time. Recent work supports periodic low-field observations occurring 10–100 Myr prior to the onset of three Phanerozoic superchrons (Shcherbakova et al. 2017, 2020; Bono *et al.* 2019; Doubrovine *et al.* 2019; Hawkins *et al.* 2019). This approximately 200 Myr quasi-periodicity in dipole strength most likely reflects mantle forcing of the geodynamo via changes in the core–mantle heat flux (Biggin *et al.* 2012). It is possible that such an oscillation extending back into the Proterozoic could account for variations observed back to at least 1100 Ma. If this were the case, then any signature of ICN and growth will be

modulated by a higher frequency mantle signal, requiring a good deal more data in poorly sampled time periods.

Whilst there remains some uncertainty over the agreement of compiled datasets with the various hypotheses, we note that these new results are consistent with an inner core which had not yet formed. A palaeofield at ~720 Ma of slightly higher strength than the recent ultralow results found ~160 Ma later in the Ediacaran (Bono *et al.* 2019) fits well on the long-term polynomial trend modelled in the same paper (Fig. 6); however, many more data are required to say anything meaningful regarding the age of ICN with any degree of certainty.

6 CONCLUSIONS

We have reported the first palaeointensity results from the middle of a 300 Myr mid-Neoproterozoic gap in the global palaeointensity database. Providing evidence of a weak time-averaged geomagnetic field at ~720 Myr, our estimates of the VDM, ranging from 3.6 to 19.3 ZAm^2 ($N \geq 3$), are acquired from six widespread dykes and one sill of the Franklin Large Igneous Province. A further four sites reporting equivalent successful results with $N < 3$ are not used to determine VDMs. Consistently low field values are observed within and between site (and method), with 39 results ranging from 1.1 to 9.9 μT. Displaying a high degree of consistency in absolute terms, site mean standard deviations are less than 3 μT. The results are also associated with high Q_{PI} values (between 5 and 9).

These new results are consistent with an inner core which had yet to form, although a severe paucity in global records remains, particularly for the Neoproterozoic era, making any meaningful conclusions regarding the age of ICN unfeasible. They do provide a real constraint at a crucial time, on recent numerical models and statistical hypotheses, and may be significant in narrowing the argument for alternative ages for ICN.

ACKNOWLEDGEMENTS

efforts in expediting samples to us and the Institute of Rock Magnetism at the University of Minnesota, USA. HCH acknowledges the help of Steve Denyszyn in the collection of samples, often under difficult weather and terrain conditions.

DATA AVAILABILITY

S. Lloyd, A. Biggin, H. Halls, M. Hill; First palaeointensity data from the cryogenian and their potential implications for inner core nucleation age; Magic Information Consortium (MagIC), 10.7288/V4/MAGIC/17065.

REFERENCES

Aubert, J., Labrosse, S. & Poitou, C., 2009. Modelling the palaeo-evolution of the geodynamo, *Geophys. J. Int.,* **179,** 1414–1428.

Biggin, A.J., Perrin, M. & Shaw, J., 2007. A comparison of a quasi-perpendicular method of absolute palaeointensity determination with other thermal and microwave techniques, *Earth planet. Sci. Lett.,* **257,** 564–581.

Biggin, A.J. *et al.*, 2012. Possible links between long-term geomagnetic variations and whole-mantle convection processes, *Nat. Geosci.,* **5,** 526–533.

Biggin, A.J. & Paterson, G.A., 2014. A new set of qualitative reliability criteria to aid inferences on palaeomagnetic dipole moment variations through geological time, *Front. Earth Sci.,* **2,** 1–9.

Biggin, A.J., Piispa, E.J., Pesonen, L.J., Holme, R., Paterson, G.A., Veikkolainen, T. & Tauxe, L., 2015. Palaeomagnetic field intensity variations suggest Mesoproterozoic inner-core nucleation, *Nature,* **526,** 245–248.

Biggin, A.J., Bono, R.K., Meduri, D.G., Sprain, C.J., Davies, C.J., Holme, R. & Doubrovine, P.V., 2020. Quantitative estimates of average geomagnetic axial dipole dominance in deep geological time, *Nat. Commun.,* **11,**

Bono, R.K., Tarduno, J.A., Nimmo, F. & Cottrell, R.D., 2019. Young inner core inferred from Ediacaran ultra-low geomagnetic field intensity, *Nat. Geosci.,* **12,** 143–147.

Bryan, S.E. & Ernst, R.E., 2008. Revised definition of Large Igneous Provinces (LIPs), *Earth-Sci. Rev.,* **86,** 175–202.

Buchan, K.L., Mertanen, S., Park, R.G., Pesonen, L.J., Elming, S.Å., Abrahamsen, N. & Bylund, G., 2000. Comparing the drift of Laurentia and Baltica in the Proterozoic: the importance of key palaeomagnetic poles, *Tectonophysics,* **319,** 167–198.

Cromwell, G., Johnson, C.L., Tauxe, L., Constable, C.G. & Jarboe, N.A., 2018. PSV10: a global data set for 0–10 Ma time-averaged field and paleosecular variation studies, *Geochem. Geophys. Geosyste.,* **19,** 1533–1558.

Davies, C., Pozzo, M., Gubbins, D. & Alfè, D., 2015. Constraints from material properties on the dynamics and evolution of Earth's core, *Nat. Geosci.,* **8,** 678–685.

,Day, R., Fuller, M. & Schmidt, V.A., 1977. Hysteresis properties of titanomagnetites: grain-size and compositional dependence, *Phys. Earth planet. Inter.,* **13,** 260–267.

Denyszyn, S.W., Halls, H.C. & Davis, D.W., 2004. A paleomagnetic, geochemical and U-Pb geochronological comparison of the Thule (Greenland) and Devon Island (Canada) dyke swarms and its relevance to the Nares Strait problem, *Polarforschung,* **74,** 63–75.

Denyszyn, S.W., Halls, H.C., Davis, D.W. & Evans, D.A.D., 2009. Paleomagnetism and U-Pb geochronology of Franklin dykes in high arctic Canada and Greenland: a revised age and paleomagnetic pole constraining block rotations in the Nares Strait region, *Can. J. Earth Sci.,* **46,** 689–705.

Doubrovine, P.V. *et al.*, 2019. Latitude dependence of geomagnetic paleosecular variation and its relation to the frequency of magnetic reversals: observations from the Cretaceous and Jurassic, *Geochem. Geophys. Geosyst.,* **20,** 1240–1279.

Driscoll, P. & Bercovici, D., 2014. On the thermal and magnetic histories of Earth and Venus: influences of melting, radioactivity, and conductivity, *Phys. Earth planet. Inter.,* **236,** 36–51.

Driscoll, P.E., 2016. Simulating 2 Ga of geodynamo history, *Geophys. Res. Lett.,* **43,** 5680–5687.

Dunlop, D., Özdemir, Ö. & Fuller, M.D., 1998. Rock magnetism: fundamentals and frontiers, *Phys. Today,* doi:10.1063/1.882466

Grappone, J.M., Biggin, A.J & Hill, M.J., 2019. Solving the mystery of the 1960 Hawaiian lava flow: implications for estimating Earth's magnetic field, *Geophys. J. Int.,* **218,** 1796–1806.

Gubbins, D., Alfè, D., Davies, C. & Pozzo, M., 2014. On core convection and the geodynamo: effects of high electrical and thermal conductivity, *Phys. Earth planet. Inter.,* **247,** 56–64.

Hawkins, L.M.A., Anwar, T., Shcherbakova, V.V., Biggin, A.J., Kravchinsky, V.A., Shatsillo, A.V. & Pavlov, V.E., 2019. An exceptionally weak Devonian geomagnetic field recorded by the Viluy Traps, Siberia, *Earth planet. Sci. Lett.,* **506,** 134–145.

Heaman, L.M., LeCheminant, A.N. & Rainbird, R.H., 1992. Nature and timing of Franklin igneous events, Canada: implications for a Late Proterozoic mantle plume and the break-up of Laurentia, *Earth planet. Sci. Lett.,* **109,** 117–131.

Hill, M.J. & Shaw, J., 1999. Palaeointensity results for historic lavas from Mt Etna using microwave demagnetization/remagnetization in a modified Thellier-type experiment, *Geophys. J. Int.,* doi:10.1046/j.1365-246X.1999.00980.x

Hill, M.J. & Shaw, J., 2000. Magnetic field intensity study of the 1960 Kilauea lava flow, Hawaii, using the microwave palaeointensity technique, *Geophys. J. Int.,* **142,** 487–504.

Hill, M.J., Gratton, M.N. & Shaw, J., 2002. A comparison of thermal and microwave palaeomagnetic techniques using lava containing laboratory induced remanence, *Geophys. J. Int.,* **151,** 157–163.

Kodama, K.P., Carnes, L.K., Tarduno, J.A. & Berti, C., 2019. Palaeointensity of the 1.3 billion-yr-old Gardar basalts, southern Greenland revisited: no evidence for onset of inner core growth, *Geophys. J. Int.,* **217,** 1974–1987.

Koker, N. De, Steinle-Neumann, G. & Vlček, V., 2012. Electrical resistivity and thermal conductivity of liquid Fe alloys at high P and T, and heat flux in Earth's core, *Proc. Natl. Acad. Sci. USA,* **109,** 4070–4073.

Konôpková, Z., McWilliams, R.S., Gómez-Pérez, N. & Goncharov, A.F., 2016. Direct measurement of thermal conductivity in solid iron at planetary core conditions, *Nature,* **534,** 99–101.

Kulakov, E.V., Smirnov, A.V. & Diehl, J.F., 2013. Absolute geomagnetic paleointensity as recorded by ∼1.09 Ga Lake Shore Traps (Keweenaw Peninsula, Michigan), *Stud. Geophys. Geod.,* **57,** 565–584.

Kulakov, E.V. *et al.*, 2019. Analysis of an updated paleointensity database (QPI-PINT) for 65–200 Ma: implications for the long-term history of dipole moment through the Mesozoic, *J. geophys. Res.,* **124,** 9999–10 022.

Labrosse, S., 2014. Thermal evolution of the core with a high thermal conductivity, *Phys. Earth planet. Inter.,* **247,** 36–55.

Landeau, M., Aubert, J. & Olson, P., 2017. The signature of inner-core nucleation on the geodynamo, *Earth planet. Sci. Lett.,* **465,** 193–204.

Nimmo, F., 2015. Thermal and compositional evolution of the core, in *Treatise on Geophysics,* 2nd edn, doi:10.1016/B978-0-444-53802-4.00160-3

O'Rourke, J.G. & Stevenson, D.J., 2016. Powering Earth's dynamo with magnesium precipitation from the core, *Nature,* **529,** 387–389.

Ohta, K., Kuwayama, Y., Hirose, K., Shimizu, K. & Ohishi, Y., 2016. Experimental determination of the electrical resistivity of iron at Earth's core conditions, *Nature,* **534,** 95–98.

Palmer, H.C., Baragar, W.R.A., Fortier, M. & Foster, J.H., 1983. Paleomagnetism of Late Proterozoic rocks, Victoria Island, Northwest Territories, Canada, *Can. J. Earth Sci.,* **20,** 1456–1469.

Park, J.K., 1994. Palaeomagnetic constraints on the position of Laurentia from middle Neoproterozoic to Early Cambrian times, *Precambrian Res.,* **69,** 95–112.

Paterson, G.A., Tauxe, L., Biggin, A.J., Shaar, R. & Jonestrask, L.C., 2014. Standard Paleointensity definitions v1.1, 0–43, Retrieved from http://www.paleomag.net/SPD/spdweb.html

Pehrsson, S.J. & Buchan, K.L., 1999. Borden dykes of Baffin Island, northwest territories: a Franklin U-Pb baddeleyite age and a paleomagnetic reinterpretation, *Can. J. Earth Sci.,* doi:10.1139/e98-091

Pozzo, M., Davies, C., Gubbins, D. & Alfè, D., 2012. Thermal and electrical conductivity of iron at Earth's core conditions, *Nature,* **485,** 355–358.

Prévot, M., 1981. Some aspects of magnetic viscosity in subaerial and submarine volcanic rocks, *Geophys. J. R. astr. Soc.,* **66,** 169–192.

Shcherbakova, V.V., Biggin, A.J., Veselovskiy, R.V., Shatsillo, A.V., Hawkins, L.M.A., Shcherbakov, V.P. & Zhidkov, G.V., 2017. Was the Devonian geomagnetic field dipolar or multipolar? Palaeointensity studies of Devonian igneous rocks from the Minusa Basin (Siberia) and the Kola Peninsula dykes, Russia, *Geophys. J. Int.,* **209,** 1265–1286.

Shcherbakova, V.V., Bakhmutov, V.G., Thallner, D., Shcherbakov, V.P., Zhidkov, G.V. & Biggin, A.J., 2020. Ultra-low palaeointensities from East European Craton, Ukraine support a globally anomalous palaeomagnetic field in the Ediacaran, *Geophys. J. Int.,* **220,** 1920–1946.

Shellnutt, J.G., Dostal, J. & Keppie, J.D., 2004. Petrogenesis of the 723 Ma Coronation sills, Amundsen basin, Arctic Canada: implications for the break-up of Rodinia, *Precambrian Res.*, **129,** 309–324.

Smirnov, A.V., Tarduno, J.A., Kulakov, E.V., McEnroe, S.A. & Bono, R.K., 2016. Palaeointensity, core thermal conductivity and the unknown age of the inner core, *Geophys. J. Int.,* **205,** 1190–1195.

Smirnov, A.V., Kulakov, E.V., Foucher, M.S. & Bristol, K.E., 2017. Intrinsic paleointensity bias and the long-term history of the geodynamo, *Sci. Adv.,* **3,** 1–8.

Sprain, C.J., Swanson-Hysell, N.L., Fairchild, L.M. & Gaastra, K., 2018. A field like today's? The strength of the geomagnetic field 1.1 billion years ago, *Geophys. J. Int.,* **213,** 1969–1983.

Suttie, N., Shaw, J. & Hill, M.J., 2010. Direct demonstration of microwave demagnetization of a whole rock sample with minimal heating, *Earth planet. Sci. Lett.,* doi:10.1016/j.epsl.2010.02.002

Tauxe, L. & Staudigel, H., 2004. Strength of the geomagnetic field in the cretaceous normal superchron: new data from submarine basaltic glass of the troodos ophiolite, *Geochem. Geophys. Geosyst.,* **5**. doi:10.1029/2003GC000635

Thellier, E. & Thellier, O., 1959. Sur l'intensite du champ magnetique terrestre dans le passe historique et geologique, *Ann. Geophys.*, **15,** 285–376.

Thomas, D.N. & Piper, J.D.A., 1992. A revised magnetostratigraphy for the Mid-Proterozoic Gardar lava succession, South Greenland, *Tectonophysics,* doi:10.1016/0040-1951(92)90172-3.

Thomas, D.N. & Piper, J.D.A., 1995. Evidence for the existence of a transitional geomagnetic field recorded in a Proterozoic lava succession, *Geophys. J. Int.* doi:10.1111/j.1365-246X.1995.tb03553.x.

Thomas, N., 1993. An integrated rock magnetic approach to the selection or rejection of ancient basalt samples for palaeointensity experiments, *Phys. Earth planet. Inter.,* **75,** 329–342.

Tsunakawa, H. & Shaw, J., 1994. The Shaw method of palaeointensity determinations and its application to recent volcanic rocks, *Geophys. J. Int.,* **118,** 781–787.

Veselovskiy, R.V. *et al.*, 2019. 1.86 Ga key paleomagnetic pole from the Murmansk craton intrusions – Eastern Murman Sill Province, NE Fennoscandia: multidisciplinary approach and paleotectonic applications, *Precambrian Res.,* **324,** 126–145.

Walton, D., Shaw, J., Share, J. & Hakes, J., 1992. Microwave demagnetization, *J. Appl. Phys.,* **71,** 1549–1551.

Yamamoto, Y., Tsunakawa, H. & Shibuya, H., 2003. Palaeointensity study of the Hawaiian 1960 lava: implications for possible causes of erroneously high intensities, *Geophys. J. Int.,* **153,** 263–276.

Zhang, Y. *et al.*, 2020. Reconciliation of experiments and theory on transport properties of iron and the geodynamo, *Phys. Rev. Lett.,* **125,** 78501, doi:10.1103/PhysRevLett.125.078501.

SUPPORTING INFORMATION

Supplementary data are available at *GJI* online.

Figure S1. *k–T* curves. Red lines, heating curve; blue lines, cooling curve; *k*, susceptibility; *T*, temperature.

Figure S2. Electron-dispersive X-ray spectroscopy (EDS) results for four thin sections: (a) BG2-3A; (b) SG3-3-B; (c) BP9-6B; (d) QA2-1B.

Figure S3. Plot showing the difference in ARM after LTD treatment normalized by maximum difference and where zero equals identical ARM in LTD and non-LTD sister specimens (17 samples across 10 sites); hence, the maximum difference is one at 0 mT. Specimen SG3-5-3B lost no remanence after LTD treatment and is not included in this plot, while specimen QA12-2A had no magnetization to lose and is also excluded.

Figure S4. Comparison of the effect of LTD treatment on successful palaeointensity results from Shaw (LTD) DHT experiments, consisting of 20 specimens across six sites.

Figure S5. (a) Specimen BP5-1A slope is fitted from 500 to 565 °C producing a palaeointensity of 1.0 µT. (b) The same specimen slope fitted from the initial step to 565 °C produces a palaeointensity of 2.6 µT. The low-temperature section of the Arai diagram corresponds to an overprint direction and could not be taken as the ChRM. The figure illustrates that the potential error from underestimation associated with selecting the high-temperature section of this two-slope Arai diagram is small.

Figure S6. Example Arai plot showing excessive 'zigzagging' in specimen SG2-13A; quantified by the β parameter.

Figure S7. Plot of direct sister specimen comparison from Shaw-DHT and Microwave methods. R^2 correlation A, full specimen correlation; R^2 correlation B, after removal of single adjacent outlier.

Table S1. Shaw experiment results. Dec, delination; Inc, inclination; *N*, number of steps; HL, lowest coercivity step used; fN, fraction of coercivity used; Alpha, alpha criteria; MAD, maximum angular deviation; LTD, low-temperature demagnetization; γ, gamma value; sA1 and sA2, slopes A1 and A2; sN, slope N; rN, R^2 correlation coefficient for slope N; sT, slopeT; rT, R^2 correlation of slope T; *F*, field intensity (µT); Class, results classification. Specimens with no data produced uninterpretable directions from the AF demagnetization of the NRM and were removed from the experiment. Missing Dec and Inc information was determined to be unreliable.

Table S2. Thellier experiment results. Column headings are defined in the selection criteria (main document, Section 3.2). AF column indicates specimens that underwent a 5 mT cleanse before each measurement step. Specimens with no results were uninterpretable.

Table S3. Microwave experiment results. Column headings are defined in the selection criteria (main document, Section 3.2)

Table S4. Data used to determine the VGP scatter. Dec, declination; Inc, inclination; Ndir, number used for direction; kdir, *k* statistic; Slat, site latitude; Slon, site longitude; Plat, unrotated VGP palaeolatitude; Plon, unrotated VGP palaeolongitude; PlatR, rotated VGP palaeolatitude; PlonR, rotated VGP palaeolongitude; DecR, declination recalculated from pole rotations for Canada and Greenland (see Section S3). Slat, Slon, Plat and Plon taken from Denyszyn *et al.* (2009). Plat and Plon for sies SG2 and NU1 are antipoles

Table S5. Potentially rejected specimens due to application of stricter selection criteria and their effect on the site mean. These original results would be rejected as a consequence of applying a stricter DRAT and CDRAT minima of 13 and 15 per cent respectively to thermal Thellier and Microwave data, and a slightly stricter slopeT of 1 ± 0.6 in Shaw-DHT data. The effect of removing these results is negligible. TH, Thellier; MW, Microwave; SH, Shaw-DHT; CRITREJECT; reason for rejection; BANC, palaeointensity result.

Table S6. QPI breakdown per site. MAG pass due to all raw data being included as a file in the submission of this paper.

Please note: Oxford University Press is not responsible for the content or functionality of any supporting materials supplied by the authors. Any queries (other than missing material) should be directed to the corresponding author for the paper.